Available online at www.sciencedirect.com
SCIENCE DIRECT®
Mechanics of Materials 35 (2003) 245–258
MECHANICS OF MATERIALS
www.elsevier.com/locate/mechmat

# The flow theory of mechanism-based strain gradient plasticity

X. Qiu [a], Y. Huang [b,*], Y. Wei [c], H. Gao [d], K.C. Hwang [a]

[a] Failure Mechanics Laboratory, Department of Engineering Mechanics, Tsinghua University, Beijing 100084, China
[b] Department of Mechanical and Industrial Engineering, University of Illinois, 1206 West Green Street, Urbana, IL 61801, USA
[c] Institute of Mechanics, Academy of Sciences, Beijing 100080, China
[d] Division of Mechanics and Computation, Stanford University, Palo Alto, CA 94305, USA

Received 7 July 2001; received in revised form 16 January 2002

**Abstract**

The flow theory of mechanism-based strain gradient (MSG) plasticity is established in this paper following the same multiscale, hierarchical framework for the deformation theory of MSG plasticity in order to connect with the Taylor model in dislocation mechanics. We have used the flow theory of MSG plasticity to study micro-indentation hardness experiments. The difference between deformation and flow theories is vanishingly small, and both agree well with experimental hardness data. We have also used the flow theory of MSG plasticity to investigate stress fields around a stationary mode-I crack tip as well as around a steady state, quasi-statically growing crack tip. At a distance to crack tip much larger than dislocation spacings such that continuum plasticity still applies, the stress level around a stationary crack tip in MSG plasticity is significantly higher than that in classical plasticity. The same conclusion is also established for a steady state, quasi-statically growing crack tip, though only the flow theory can be used because of unloading during crack propagation. This significant stress increase due to strain gradient effect provides a means to explain the experimentally observed cleavage fracture in ductile materials [J. Mater. Res. 9 (1994) 1734; Scripta Metall. Mater. 31 (1994) 1037; Interface Sci. 3 (1996) 169].


## 1. Introduction

Micro-indentation hardness experiments have repeatedly shown that the hardness of metallic materials increases by a factor of two or even three as the depth of indentation decreases to microns or sub-microns (e.g., Nix, 1989, 1997; de Guzman et al., 1993; Stelmashenko et al., 1993; Atkinson, 1995; Ma and Clarke, 1995; Poole et al., 1996; McElhaney et al., 1998; Suresh et al., 1999; Tymiak et al., 2001). Similar size dependence of plastic behavior of materials at the micron scale has also been observed in micro-torsion (Fleck et al., 1994) and micro-bend experiments (Stolken and Evans, 1998) of thin metallic wires and foils, as well as in particle-reinforced metal-matrix composite materials (Lloyd, 1994; Nan and Clarke, 1996; Zhu et al., 1997). Direct dislocation simulations have also shown strong size dependence of metallic material at the micron scale under various loading conditions (van der Giessen and Needleman, 1995; Cleveringa et al., 1997, 1998, 1999a,b, 2000; Needleman, 2000).

* Corresponding author. Tel.: +1-217-265-5072; fax: +1-217-244-6534.
*E-mail address:* huang9@uiuc.edu (Y. Huang).

0167-6636/03/$ - see front matter © 2002 Elsevier Science Ltd. All rights reserved.
PII: S0167-6636(02)00274-0

Classical plasticity theories do not possess internal material lengths and therefore cannot explain the observed size dependence of material behavior. Accordingly, strain gradient plasticity theories have been proposed (e.g., Fleck and Hutchinson, 1993, 1997; Fleck et al., 1994; Gao et al., 1999b; Huang et al., 1999, 2000a,b; Shu and Fleck, 1999; Acharya and Bassani, 2000; Acharya and Beaudoin, 2000; Dai and Parks, 2002) based on the notion of geometrically necessary dislocations (Nye, 1953; Cottrell, 1964; Ashby, 1970; Arsenlis and Parks, 1999; Gurtin, 2000), and are intended for applications to materials and structures whose dimension controlling plastic deformation falls into the range of microns and submicrons. There also exist earlier works on strain gradient plasticity that were proposed to avoid a spurious solution for the localized zone and an excessive mesh dependence in classical plasticity (e.g., Aifantis, 1984, 1992; Lasry and Belytschko, 1988; Zbib and Aifantis, 1988; Muhlhaus and Aifantis, 1991; de Borst and Muhlhaus, 1992; Sluys et al., 1993). One strain gradient theory, namely mechanism-based strain gradient (MSG) plasticity (Gao et al., 1999b; Huang et al., 1999, 2000a,b), is established from a multiscale, hierarchical framework to connect with the Taylor model in dislocation mechanics (Taylor, 1934, 1938). It agrees well with McElhaney et al.'s (1998)'s micro-indentation experiments of bulk copper (see Huang et al., 2000b) and Saha et al.'s (2001) indentation experiments of aluminum thin film on a glass substrate, with Fleck et al.'s (1994) micro-torsion and Stolken and Evans' (1998) micro-bend experiments (see Gao et al., 1999a), and with Lloyd's (1994) metal-matrix composite (see Xue et al., 2002a). It has also been successfully applied to study a few important problems at the micron and submicron scales, including micro-electro-mechanical systems (Xue et al., 2002b), plastic flow localization (Hao et al., 2000; Shi et al., 2000b), and fracture (Shi et al., 2000a; Jiang et al., 2001). However, the present MSG plasticity theory is a deformation theory which has not accounted for elastic unloading nor for non-proportional deformation as in crack propagation.

The purpose of this paper is to develop the flow theory of MSG plasticity. The flow theory is established in Section 2 following the same multiscale, hierarchical framework to connect with the Taylor model in dislocation mechanics (Taylor, 1934, 1938). Numerical methods for the flow theory of MSG plasticity have been developed and used to study the strain gradient effect in micro-indentation hardness experiments and in the asymptotic field around a stationary crack tip in Sections 3 and 4, respectively. The quasi-static, steady-state propagation of a mode-I crack is investigated in Section 5.

## 2. The flow theory of MSG plasticity

Fig. 1 shows the multiscale, hierarchical framework adopted by Gao et al. (1999b) to construct the theory of MSG plasticity from the Taylor model in dislocation mechanics (Taylor, 1934, 1938). We distinguish the microscale on which dislocation activities are governed by the Taylor dislocation model from the mesoscale on which strain gradient plasticity theories are constructed. On the microscale, the scale of analysis is small compared with the length over which the strain field varies, and dislocation activities are described by the slip of statistically stored dislocations in a background of geometrically necessary dislocations which influence the microscale flow stress

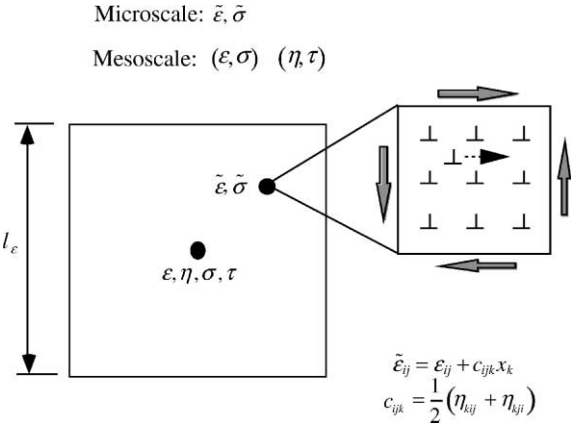


Fig. 1. A schematic diagram of the multiscale framework to connect the mesoscale theory of strain gradient plasticity to the Taylor dislocation model on the microscale.

according to the Taylor model. At this level of analysis, the stress and strain tensors are defined in the classical sense, and are denoted by $\tilde{\boldsymbol{\sigma}}$ and $\tilde{\boldsymbol{\epsilon}}$, respectively. Concepts associated with strain gradient plasticity, such as the higher-order stress tensor $\boldsymbol{\tau}$ and strain gradient tensor $\boldsymbol{\eta}$, are introduced at a higher level of analysis, which will be referred to as the mesoscale analysis. Here the terminology "mesoscale" is adopted because the continuum strain gradient plasticity theory is formulated based on dislocation activities on a subscale which we have referred to as the "microscale". The stress and strain tensors at the mesoscale are denoted by $\boldsymbol{\sigma}$ and $\boldsymbol{\epsilon}$, respectively, while the strain gradient tensor $\boldsymbol{\eta}$ is defined in terms of the displacement $\boldsymbol{u}$ by

$$\eta_{ijk} = u_{k,ij} = \epsilon_{ik,j} + \epsilon_{kj,i} - \epsilon_{ij,k}. \tag{1}$$

The microscale picture of Taylor hardening is connected to the mesoscale picture of strain gradient plasticity through the mesoscale cell shown in Fig. 1. From kinematics analysis (Gao et al., 1999b), the microscale strain tensor in the cell is related to the mesoscale strain and strain gradient by

$$\tilde{\epsilon}_{ij} = \epsilon_{ij} + \tfrac{1}{2}(\eta_{kij} + \eta_{kji})\tilde{x}_k, \tag{2}$$

where $\tilde{x}_k$ denotes the local Cartesian coordinate with origin at the mesoscale cell center (Fig. 1). The right hand side of (2) can be viewed as the first two terms in the power series expansion of microscale strain within the mesoscale cell. Therefore, the mesoscale cell size $l_\epsilon$ (Fig. 1) must be small compared to the internal material length in strain gradient plasticity in order to ensure the accuracy of (2).

From energetic considerations, equality of total work at the two scales requires (Gao et al., 1999b)

$$\int_{V_{\text{cell}}} \tilde{\sigma}_{ij}\delta\tilde{\epsilon}_{ij}\,\mathrm{d}v = (\sigma_{ij}\delta\epsilon_{ij} + \tau_{ijk}\delta\eta_{ijk})V_{\text{cell}}, \tag{3}$$

where integration is over the mesoscale cell $V_{\text{cell}}$, and $\delta$ stands for the virtual variation.

By substituting (2) into (3), we obtain the mesoscale symmetric stress $\sigma_{ij}$ $(=\sigma_{ji})$ and symmetric higher-order stress $\tau_{ijk}$ $(=\tau_{jik})$ in terms of the microscale stress $\tilde{\sigma}_{ij}$ in the cell,

$$\sigma_{ij} = \frac{1}{V_{\text{cell}}}\int_{V_{\text{cell}}} \tilde{\sigma}_{ij}\,\mathrm{d}v, \tag{4}$$

$$\tau_{ijk} = \frac{1}{2V_{\text{cell}}}\int_{V_{\text{cell}}} (\tilde{\sigma}_{ki}x_j + \tilde{\sigma}_{kj}x_i)\,\mathrm{d}v. \tag{5}$$

It becomes clear that, once the microscale stress–strain relation ($\tilde{\boldsymbol{\sigma}}$ versus $\tilde{\boldsymbol{\epsilon}}$) is known, the constitutive law of strain gradient plasticity is determined since the mesoscale stress $\boldsymbol{\sigma}$ and higher-order stress $\boldsymbol{\tau}$ can be obtained from the mesoscale strain $\boldsymbol{\epsilon}$ and strain gradient $\boldsymbol{\eta}$ via (4), (5) and (2). The microscale stress–strain relation is discussed in the following.

### 2.1. Microscale analysis

The associative rule of plastic flow normality holds on the microscale if dislocation slip is proportional to the resolved Schmid stress (Rice, 1970, 1971),

$$\frac{\dot{\tilde{\epsilon}}^{\text{p}}_{ij}}{\dot{\tilde{\epsilon}}^{\text{p}}} = \frac{3\tilde{\sigma}'_{ij}}{2\tilde{\sigma}_{\text{e}}} \quad \text{if } \dot{\tilde{\epsilon}}^{\text{p}} > 0, \tag{6}$$

where $\dot{\tilde{\epsilon}}^{\text{p}}_{ij}$ is the microscale plastic strain rate, $\dot{\tilde{\epsilon}}^{\text{p}} = \sqrt{(2/3)\dot{\tilde{\epsilon}}^{\text{p}}_{ij}\dot{\tilde{\epsilon}}^{\text{p}}_{ij}}$ the effective plastic strain rate, $\tilde{\sigma}'_{ij}$ the microscale deviatoric stress, and $\tilde{\sigma}_{\text{e}} = \sqrt{(3/2)\tilde{\sigma}'_{ij}\tilde{\sigma}'_{ij}}$ the effective stress. The total strain rate is composed of the elastic part $\dot{\tilde{\epsilon}}^{\text{e}}_{ij}$ and plastic part $\dot{\tilde{\epsilon}}^{\text{p}}_{ij}$,

$$\dot{\tilde{\epsilon}}_{ij} = \dot{\tilde{\epsilon}}^{\text{e}}_{ij} + \dot{\tilde{\epsilon}}^{\text{p}}_{ij} = \frac{1}{2\mu}\dot{\tilde{\sigma}}'_{ij} + \frac{1}{9K}\dot{\tilde{\sigma}}_{kk}\delta_{ij} + \dot{\tilde{\epsilon}}^{\text{p}}_{ij}, \tag{7}$$

where the elastic strain rate is given in terms of the stress rate $\dot{\tilde{\sigma}}_{ij}$ via the linear elastic constitutive relation, $\mu$ and $K$ are elastic shear and bulk moduli, respectively.

The yield criterion on the microscale is (Nix and Gao, 1998; Gao et al., 1999b)

$$\tilde{\sigma}_{\text{e}} = \tilde{\sigma}, \tag{8}$$

where $\tilde{\sigma}$ is the microscale flow stress derived from the Taylor model in dislocation mechanics to account for the effect of geometrically necessary dislocations, and is given by

$$\tilde{\sigma}^2 = \sigma^2_{\text{ref}} f^2_{\text{p}}(\bar{\epsilon}^{\text{p}}) + 18\alpha^2\mu^2 b\eta. \tag{9}$$

[It is important to distinguish $\tilde{\sigma}$ for (scalar) flow stress from $\tilde{\boldsymbol{\sigma}}$ for stress tensor.] Here $\sigma = \sigma_{\text{ref}} f_{\text{p}}(\epsilon^{\text{p}})$

gives the relation between stress and plastic strain in uniaxial tension, $\sigma_{\text{ref}}$ is a reference stress; $\tilde{\epsilon}^{\text{p}} = \int_0^t \dot{\tilde{\epsilon}}^{\text{p}}\,\mathrm{d}t$ is the non-decreasing accumulative plastic strain at the microscale; $b$ is the Burgers vector; $\alpha$ is an empirical coefficient in the Taylor model and is between 0.1 and 0.5 (Taylor, 1934, 1938); and $\eta$ is the mesoscale effective strain gradient, which is related to the density of geometrically necessary dislocations, $\rho_{\text{G}}$, by (Gao et al., 1999b; Huang et al., 2000b)

$$\eta = \rho_{\text{G}} b/2. \tag{10}$$

Gao et al. (1999b) have developed dislocation models to determine the effective strain gradient $\eta$ in terms of deviatoric strain gradient $\eta'_{ijk}$ as

$$\eta = \sqrt{\tfrac{1}{4}\eta'_{ijk}\eta'_{ijk}}, \tag{11}$$

where $\eta'_{ijk} = \eta_{ijk} - \eta^H_{ijk}$, and the volumetric part of strain gradient is

$$\eta^H_{ijk} = \tfrac{1}{4}(\delta_{ik}\eta_{jpp} + \delta_{jk}\eta_{ipp}). \tag{12}$$

The strain tensor is decomposed to the elastic and plastic strains, and the plastic strain results from the slip of statistically stored dislocations. The strain gradient tensor, however, is not decomposed in the same way because it reflects the effect of geometrically necessary dislocations, and the latter accommodate the non-uniformity of deformation.

The critical difference between constitutive relations (6)–(10) and those of classical $J_2$-flow plasticity theory is the microscale flow stress in (9), which accounts for the effect of geometrically necessary dislocations via the mesoscale strain gradient term to increase the flow stress. Because of the mesoscale strain gradient term in the microscale flow stress, (6)–(10) are not a self-contained constitute model at the microscale. In the following we derive the mesoscale flow theory of MSG plasticity by averaging the microscale constitutive relations (6)–(10) in the mesoscale cell.

### 2.2. Mesoscale analysis: zeroth-order average

The average of any microscale variable $\tilde{p}$ in the mesoscale cell is defined by

$$p^{(0)} = \frac{1}{V_{\text{cell}}}\int_{V_{\text{cell}}} \tilde{p}\,\mathrm{d}v,$$

which is also called the zeroth-order average of $\tilde{p}$. It is obvious from (2) and (4) that the zeroth-order average of microscale strain $\tilde{\boldsymbol{\epsilon}}$ and stress $\tilde{\boldsymbol{\sigma}}$ are the mesoscale strain $\boldsymbol{\epsilon}$ and stress $\boldsymbol{\sigma}$, respectively. It is straightforward to show that the zeroth-order average of (7) gives the mesoscale strain rate

$$\dot{\epsilon}_{ij} = \dot{\epsilon}^{\text{e}}_{ij} + \dot{\epsilon}^{\text{p}}_{ij} = \frac{1}{2\mu}\dot{\sigma}'_{ij} + \frac{1}{9K}\dot{\sigma}_{kk}\delta_{ij} + \dot{\epsilon}^{\text{p}}_{ij}, \tag{13}$$

where $\dot{\sigma}_{ij}$ is the mesoscale stress rate, $\dot{\sigma}'_{ij} = \dot{\sigma}_{ij} - (1/3)\dot{\sigma}_{kk}\delta_{ij}$ is the deviatoric part of $\dot{\sigma}_{ij}$, and the mesoscale plastic strain rate $\dot{\epsilon}^{\text{p}}_{ij}$ is obtained from the average of (6) as

$$\dot{\epsilon}^{\text{p}}_{ij} = \frac{3\sigma'_{ij}}{2\sigma_{\text{e}}}\dot{\epsilon}^{\text{p}} \quad \text{if } \dot{\epsilon}^{\text{p}} > 0. \tag{14}$$

Here $\sigma'_{ij}$, $\sigma_{\text{e}} = \sqrt{(3/2)\sigma'_{ij}\sigma'_{ij}}$ and $\dot{\epsilon}^{\text{p}} = \sqrt{(2/3)\dot{\epsilon}^{\text{p}}_{ij}\dot{\epsilon}^{\text{p}}_{ij}}$ are the mesoscale deviatoric stress, effective stress and effective plastic strain rate, respectively. The zeroth-order average of (8) gives the mesoscale yield criterion

$$\sigma_{\text{e}} = \sigma, \tag{15}$$

where the mesoscale flow stress $\sigma$ is obtained from the zeroth-order average of (9) as

$$\sigma^2 = \sigma^2_{\text{ref}} f^2_{\text{p}}(\epsilon^{\text{p}}) + 18\alpha^2\mu^2 b\eta \tag{16}$$

and $\epsilon^{\text{p}} = \int_0^t \dot{\epsilon}^{\text{p}}\,\mathrm{d}t$ is the non-decreasing accumulative equivalent plastic strain on the mesoscale. [It is important to distinguish $\sigma$ for (scalar) flow stress from $\boldsymbol{\sigma}$ for stress tensor.]

The rate form of (15) and (16) during plastic loading ($\dot{\epsilon}^{\text{p}} > 0$) gives

$$\sigma_{\text{e}}\dot{\sigma}_{\text{e}} = \sigma^2_{\text{ref}} f_{\text{p}}(\epsilon^{\text{p}}) f'_{\text{p}}(\epsilon^{\text{p}})\dot{\epsilon}^{\text{p}} + 9\alpha^2\mu^2 b\dot{\eta}, \tag{17}$$

where

$$\dot{\boldsymbol{\eta}} = \frac{\eta'_{ijk}}{4\eta}\dot{\eta}'_{ijk} = \frac{\eta'_{ijk}}{4\eta}\dot{\eta}_{ijk}. \tag{18}$$

From (13), (14) and (17), the effective plastic strain rate $\dot{\epsilon}^{\text{p}}$ is found in terms of the rates of mesoscale strain and strain gradient,

$$\dot{\epsilon}^{\text{p}} = \frac{1}{1+a}\frac{1}{\sigma}(\sigma'_{ij}\dot{\epsilon}_{ij} - 3\alpha^2\mu b\dot{\eta}), \tag{19}$$

where the mesoscale yield criterion (15) has been used, $\dot{\eta}$ is given in (18), and

$$a = \frac{\sigma_{\mathrm{ref}}^2 f_{\mathrm{p}}(\epsilon^{\mathrm{p}}) f_{\mathrm{p}}'(\epsilon^{\mathrm{p}})}{3\mu\sigma}. \tag{20}$$

The mesoscale stress rate is then given by

$$\dot{\sigma}_{ij} = K\dot{\epsilon}_{kk}\delta_{ij} + 2\mu\left(\dot{\epsilon}'_{ij} - \frac{3\sigma'_{ij}}{2\sigma}\dot{\epsilon}^{\mathrm{p}}\right). \tag{21}$$

### 2.3. Mesoscale analysis: first-order average

In order to systematically obtain the constitutive relation between strain gradient and higher-order stress, we define the first-order average of any microscale variable $\tilde{p}$ within the mesoscale cell by

$$p_{\mathrm{m}}^{(1)} = \frac{1}{V_{\mathrm{cell}}}\int_{V_{\mathrm{cell}}} \tilde{p}\tilde{x}_{\mathrm{m}}\,\mathrm{d}v,$$

where $\tilde{x}_{\mathrm{m}}$ denotes the local Cartesian coordinate with origin at the mesoscale cell center. It can be shown from (2) and (5) that the first-order average of microscale strain $\tilde{\boldsymbol{\epsilon}}$ and stress $\tilde{\boldsymbol{\sigma}}$ are proportional to strain gradient $\boldsymbol{\eta}$ and higher-order stress $\boldsymbol{\tau}$ on the mesoscale, respectively. The first-order average of the yield criterion (8) and flow stress (9) gives

$$\begin{aligned} 3\sigma'_{ij}(\tau_{kij} + \tau_{kji} - \tau_{ijk}) &= \sigma_{\mathrm{ref}}^2 f_{\mathrm{p}}(\epsilon^{\mathrm{p}}) f_{\mathrm{p}}'(\epsilon^{\mathrm{p}}) \\ &\times \int_0^t \frac{\sigma'_{ij}}{\sigma}\left[\frac{l_\epsilon^2}{12}(\dot{\eta}_{kij} + \dot{\eta}_{kji}) - \frac{\dot{\tau}_{kij} + \dot{\tau}_{kji} - \dot{\tau}_{ijk}}{\mu}\right]\mathrm{d}t, \end{aligned} \tag{22}$$

where $l_\epsilon$ is the mesoscale cell size (Fig. 1), and is given by $l_\epsilon = 10(\mu/\sigma_{\mathrm{Y}})b$, (Gao et al., 1999b; Huang et al., 1999, 2000a,b), and $\sigma_{\mathrm{Y}}$ is the yield stress in uniaxial tension. The rate form of (22) during plastic loading becomes

$$\begin{aligned} &(1+a)\sigma'_{ij}(\dot{\tau}_{kij} + \dot{\tau}_{kji} - \dot{\tau}_{ijk}) \\ &\quad = ac\sigma'_{ij}(\dot{\eta}_{kij} + \dot{\eta}_{kji}) - (\tau_{kij} + \tau_{kji} - \tau_{ijk})\dot{\sigma}'_{ij} + eg_k\dot{\epsilon}^{\mathrm{p}}, \end{aligned} \tag{23}$$

where $a$ is given in (20),

$$\begin{aligned} c &= \frac{\mu l_\epsilon^2}{12}, \quad e = \frac{f_{\mathrm{p}}'(\epsilon^{\mathrm{p}})}{f_{\mathrm{p}}(\epsilon^{\mathrm{p}})} + \frac{f_{\mathrm{p}}''(\epsilon^{\mathrm{p}})}{f_{\mathrm{p}}'(\epsilon^{\mathrm{p}})}, \\ g_k &= \sigma'_{ij}(\tau'_{kij} + \tau'_{kji} - \tau'_{ijk}). \end{aligned} \tag{24}$$

The first-order average of microscale strain rate in (6) and (7), in conjunction with the mesoscale higher-order stress in (5), gives the increment of higher-order stress at the mesoscale,

$$\begin{aligned} \dot{\tau}_{ijk} &= c\left[\dot{\eta}_{ijk} + \frac{1}{2}(\dot{\eta}_{kij} + \dot{\eta}_{kji}) + \left(\frac{2K}{\mu} - \frac{4}{3}\right)\dot{\eta}_{ijk}^H\right] \\ &\quad - \frac{3\sigma'_{mn}}{2\sigma^2}\frac{c}{1+a}(\sigma'_{ki}\dot{\eta}_{jmn} + \sigma'_{kj}\dot{\eta}_{imn}) \\ &\quad - \frac{3}{4\sigma^2}\frac{1}{1+a}\Big[\sigma'_{ki}(\tau_{jmn} + \tau_{jnm} - \tau_{mnj}) \\ &\qquad + \sigma'_{kj}(\tau_{imn} + \tau_{inm} - \tau_{mni})\Big]\dot{\sigma}'_{mn} \\ &\quad + \frac{3}{4\sigma^2}\left(\frac{3\mu}{\sigma} + \frac{e}{1+a}\right)\Big[\sigma'_{ki}g_j + \sigma'_{kj}g_i\Big]\dot{\epsilon}^{\mathrm{p}} \\ &\quad - \frac{3\mu}{\sigma}\left(\tau_{ijk} - \frac{Kl_\epsilon^2}{6}\eta_{ijk}^H\right)\dot{\epsilon}^{\mathrm{p}}. \end{aligned} \tag{25}$$

### 2.4. Summary of constitutive law and equilibrium equations

The mesoscale constitutive relations (21) and (25) provide the rates of stress and higher-order stress in terms of the rates of strain and strain gradient during plastic loading. In order to account for elastic unloading, (21) and (25) are written as

$$\dot{\sigma}_{ij} = K\dot{\epsilon}_{kk}\delta_{ij} + 2\mu\left(\dot{\epsilon}'_{ij} - \alpha'\frac{3\sigma'_{ij}}{2\sigma}\dot{\epsilon}^{\mathrm{p}}\right), \tag{26}$$

$$\begin{aligned} \dot{\tau}_{ijk} &= c\left[\dot{\eta}_{ijk} + \frac{1}{2}(\dot{\eta}_{kij} + \dot{\eta}_{kji}) + \left(\frac{2K}{\mu} - \frac{4}{3}\right)\dot{\eta}_{ijk}^H\right] \\ &\quad - \alpha'\frac{3\sigma'_{mn}}{2\sigma^2}\frac{c}{1+a}(\sigma'_{ki}\dot{\eta}_{jmn} + \sigma'_{kj}\dot{\eta}_{imn}) \\ &\quad - \alpha'\frac{3}{4\sigma^2}\frac{1}{1+a}\Big[\sigma'_{ki}(\tau_{jmn} + \tau_{jnm} - \tau_{mnj}) \\ &\qquad + \sigma'_{kj}(\tau_{imn} + \tau_{inm} - \tau_{mni})\Big]\dot{\sigma}'_{mn} \\ &\quad + \alpha'\frac{3}{4\sigma^2}\left(\frac{3\mu}{\sigma} + \frac{e}{1+a}\right)\Big[\sigma'_{ki}g_j + \sigma'_{kj}g_i\Big]\dot{\epsilon}^{\mathrm{p}} \\ &\quad - \alpha'\frac{3\mu}{\sigma}\left(\tau_{ijk} - \frac{Kl_\epsilon^2}{6}\eta_{ijk}^H\right)\dot{\epsilon}^{\mathrm{p}}, \end{aligned} \tag{27}$$

where $\dot{\epsilon}^{\mathrm{p}}$ is given by (19),

$$\begin{aligned} \alpha' &= 0 \quad \text{if } \sigma_{\mathrm{e}} < \sigma, \text{ or } \sigma_{\mathrm{e}} = \sigma \quad \text{and} \quad \dot{\epsilon}^{\mathrm{p}} = 0, \\ &= 1 \quad \text{if } \sigma_{\mathrm{e}} = \sigma \quad \text{and} \quad \dot{\epsilon}^{\mathrm{p}} > 0. \end{aligned} \tag{28}$$

The equilibrium equations in the incremental form are

$$\dot{\sigma}_{ik,i} - \dot{\tau}_{ijk,ij} + \dot{f}_k = 0, \tag{29}$$

where $\dot{f}_k$ is the increment of body force. The increments of stress traction $\dot{t}_k$ and higher-order stress traction $\dot{r}_k$ on the surface are

$$\dot{t}_k = n_i(\dot{\sigma}_{ik} - \dot{\tau}_{ijk,j}) - D_j(n_i\dot{\tau}_{ijk}) + n_i n_j \dot{\tau}_{ijk}(D_q n_q), \tag{30}$$

$$\dot{r}_k = n_i n_j \dot{\tau}_{ijk}, \tag{31}$$

where $n_i$ is the unit normal to the surface, and

$$D_j = (\delta_{jk} - n_j n_k)\frac{\partial}{\partial x_k}$$

is the surface gradient operator.

Gao et al. (1999b) pointed out that the flow theory and deformation theory of MSG plasticity become identical for an incompressible solid under proportional deformation, i.e., the displacement can be written as $\boldsymbol{u}(x,t) = \lambda(t)\boldsymbol{u}_0(x)$. However, proportional deformation does not lead to proportional stressing in MSG plasticity, $\boldsymbol{\sigma}(x,t) \neq \lambda'(t)\boldsymbol{\sigma}_0(x)$, because the flow stress $\sigma$ in (16) is non-homogeneous with respect to the strain and strain gradient. For pure bending, pure torsion and growth of a microvoid in an incompressible solid, deformation is proportional so that the flow theory gives the same results as the deformation theory does (Huang et al., 2000a). For micro-indentation experiments, Huang et al. (2000b) used the deformation theory of MSG plasticity to investigate the depth dependence of indentation hardness, and found excellent agreement between MSG plasticity and experimental data. However, deformation in micro-indentation hardness experiments is not strictly proportional (even for monotonically increasing loads). Therefore, we use the flow theory of MSG plasticity to simulate micro-indentation hardness experiments in Section 3. Similarly, we use the flow theory of MSG plasticity to investigate the asymptotic field around a stationary crack tip in Section 4 and quasi-static, steady-state crack propagation in Section 5.

## 3. Numerical studies of micro-indentation experiments

Huang et al. (2000b) used the same indentation model of Begley and Hutchinson (1998) to simulate micro-indentation hardness experiments with the deformation theory of MSG plasticity. We follow the same approach in the present study, except the deformation theory of MSG plasticity is replaced by the flow theory in Section 2. Accordingly, we only briefly summarize the indentation model, and refer readers to Begley and Hutchinson (1998) and Huang et al. (2000b) for details.

We simulate an axisymmetric conical indenter with the half cone angle of 72°, corresponding to a Vickers indenter. Friction between the indenter and indented material is neglected. Following Begley and Hutchinson (1998) and Huang et al. (2000b), the normal displacement is prescribed over the contact area between the indenter and indented material, while the higher-order stress tractions vanish on the boundary. For a given indentation displacement, the contact radius is obtained iteratively to satisfy the requirement of vanishing normal stress traction at the periphery of contact. The hardness is defined by the ratio of contact force to contact area, where contact force is the total force of all nodes within the contact area in the finite element analysis.

Finite element method for the flow theory of MSG plasticity is established from the principle of virtual work, and is the same as that for Fleck and Hutchinson's (1997) general theory of strain gradient of plasticity (e.g., Begley and Hutchinson, 1998; Shu et al., 1999) except the constitutive law is replaced by that of MSG plasticity. Several elements that have been used to study the strain gradient effect (both rotation and stretch gradients of deformation) include the $C_1$ element (Begley and Hutchinson, 1998; Huang et al., 2000b), hybrid element (Shu et al., 1999; Huang et al., 2000b), and higher-order element (Wei and Hutchinson, 1997; Huang et al., 2000b). These elements are used in

the present study of micro-indentation hardness experiments.

We have taken the following material parameters from McElhaney et al.'s (1998) micro-indentation experiments for polycrastalline copper: Burgers vector $b = 0.255$ nm, shear modulus $\mu = 42$ GPa, Poisson's ratio $\nu = 0.3$, plastic work hardening exponent $N = 0.3$, which is consistent with the hardening exponent reported in prior experiments (McLean, 1962; Fleck et al., 1994). The uniaxial stress–strain relation for copper is

$$\sigma = 688\epsilon^{0.3}\ \text{MPa} = 688\left(\frac{\sigma}{E} + \epsilon^{\text{p}}\right)^{0.3}\ \text{MPa}, \qquad (32)$$

where the total strain $\epsilon$ is composed of the elastic part, $\sigma/E$, and plastic part $\epsilon^{\text{p}}$, and $E$ is the elastic modulus. The above equation gives an implicit relation $\sigma = \sigma_{\text{ref}} f_{\text{p}}(\epsilon^{\text{p}})$ governing stress and plastic strain

$$\sigma_{\text{ref}} f_{\text{p}}(\epsilon^{\text{p}}) = 688\left[\frac{\sigma_{\text{ref}}}{E} f_{\text{p}}(\epsilon^{\text{p}}) + \epsilon^{\text{p}}\right]^{0.3}\ \text{MPa}. \qquad (33)$$

For a large depth of indentation, the strain gradient effect is insignificant. The corresponding hardness, denoted by $H_0$, does not display any size dependence and is consistent with predictions by classical plasticity. Accordingly, $H_0$ depends on the uniaxial stress–strain relation, and has nothing to do with the strain gradient effect. In fact, we have determined the reference stress of 688 MPa in (32) in order to fit the experimentally reported value of $H_0 = 834$ MPa (McElhaney et al., 1998). It should be pointed out that this value of 688 MPa is larger than that reported by Huang et al. (2000b) because the latter has neglected elastic compressibility of the solid.

Fig. 2 presents the micro-indentation hardness predicted by the flow theory of MSG plasticity, $(H/H_0)^2$, versus inverse of indentation depth, $1/h$, for polycrystalline copper, where $H$ is the micro-indentation hardness, $h$ the depth of indentation, and $H_0 = 834$ MPa the indentation hardness for large $h$. The empirical coefficient $\alpha$ in the Taylor model is taken as $\alpha = 0.30$, which is in the correct range but is smaller than that reported by Huang et al. (2000b) because the latter neglected elastic compressibility of the solid. The difference between the reference stress 688 MPa and Taylor coefficient

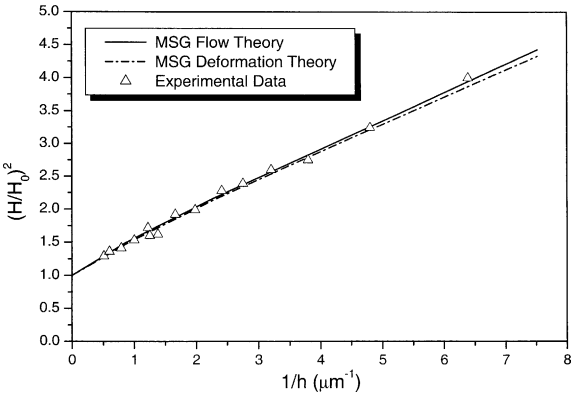


Fig. 2. The square of micro-indentation hardness, $H^2$, versus the inverse of indentation depth, $1/h$, predicted by flow and deformation theories of MSG plasticity and the experimental data of McElhaney et al. (1998); shear modulus $\mu = 42$ GPa, Possion's ration $\nu = 0.3$, and the uniaxial stress–strain relation $\sigma = 688\epsilon^{0.3}$ MPa, which gives the indentation hardness $H_0 = 834$ MPa for a large depth of indentation; the Burger vector $b = 0.255$ μm, and the Taylor coefficient $\alpha = 0.30$.

$\alpha = 0.30$ for a compressible solid and their counterparts reported in Huang et al. (2000b) for an imcompressible solid indicates that the elastic compressibility, or equivalently, the volumetric deformation, is important in the study of micro-indentation experiments and must be accounted for.

The micro-indentation hardness data reported by McElhaney et al. (1998) for polycrystalline copper are presented in Fig. 2 for comparison. The micro-indentation hardness predicted by the deformation theory of MSG plasticity is also shown in order to examine the difference between flow and deformation theories. The same set of material parameters (e.g., $\sigma_{\text{ref}} = 688$ MPa and $\alpha = 0.30$) is used. It is observed that the difference between flow and deformation theories of MSG plasticity is rather small. This is not surprising since the loading increases monotonically in micro-indentation hardness experiments. Moreover, both theories agree very well with experimental data over a wide range of indentation depth, from one tenth of a micron to several microns, indicating that MSG plasticity theories are capable of accurately characterizing plastic deformation of metallic materials at the micron and submicron scales.

## 4. Fracture analysis of a stationary mode-I crack

Jiang et al. (2001) used the deformation theory of MSG plasticity to study the stress field around a stationary mode-I crack tip. They established that, at a distance close to crack tip but still more than one order of magnitude larger than the average dislocation spacing so that continuum plasticity still applies, the stress level in MSG plasticity is significantly larger than that in classical plasticity. We use the flow theory of MSG plasticity to investigate the same problem in this section.

We have taken a circular domain of radius $10^3 l$ centered at the crack tip in our plane-strain finite element analysis, where

$$l = 18\alpha^2 \left( \frac{\mu}{\sigma_{\text{ref}}} \right)^2 b \tag{34}$$

is the internal material length in strain gradient plasticity (see (16)). Very fine mesh is used near the crack tip, around which the size of the smallest element is less than $10^{-3} l$. Mesh refinement and comparison of results from different finite elements have ensured that the numerical results are accurate.

Crack faces remain traction-free. The classical mode-I elastic $K$ field is imposed on the outer boundary of the domain (of radius $10^3 l$), with the remote applied stress intensity factor increasing monotonically such that there is no unloading.

Stresses are normalized by the yield stress $\sigma_Y$ and depend on the following non-dimensional parameters as

$$\frac{\sigma_{ij}}{\sigma_Y} = f_{ij}\left( \frac{r}{l}, \theta, N, \frac{\sigma_Y}{E}, v, \frac{K_I}{\sigma_Y l^{1/2}} \right), \tag{35}$$

where the distance $r$ to the crack tip is normalized by the internal material length $l$ in (34), $\theta$ is the polar angle, material parameters include the plastic work hardening exponent $N$, yield stress $\sigma_Y$, elastic modulus $E$, and Possion's ration $v$, and $K_I$ is the remote applied elastic stress intensity factor. The normalized stresses do not depend explicitly on the internal material length $l$, nor on the Taylor coefficient $\alpha$. Unless otherwise specified, we focus on stresses ahead of the crack tip at the polar angle $\theta = 1.0143°$, and the following set of non-dimensional material properties

$$N = 0.2, \quad \frac{\sigma_Y}{E} = 0.2\%, \quad v = 0.3. \tag{36}$$

Fig. 3 shows the normalized effective stress, $\sigma_e/\sigma_Y$, versus non-dimensional distance ahead of the crack tip, $r/l$, at polar angle $\theta = 1.0143°$. Results are presented for both flow and deformation theories of MSG plasticity, as well as the classical flow theory of plasticity (i.e., without strain gradient effect). Material properties are given in (36), while the remote applied stress intensity factor is $K_I/\sigma_Y l^{1/2} = 20$. It is observed that the difference between two theories of MSG plasticity is vanishingly small. Therefore, the deformation theory of MSG plasticity characterizes the stationary crack tip field as accurate as the flow theory does, even though deformation near the stationary crack tip is not strictly proportional. It is also seen that all three curves intercept with the horizontal line $\sigma_e/\sigma_Y = 1$ at the same distance (slightly larger than $10l$) to the crack tip, indicating that the plastic zone size is basically independent of the strain gradient effect. This is consistent with Wei and Hutchinson's (1997) observation in the study of crack tip field by the phenomenological theory of

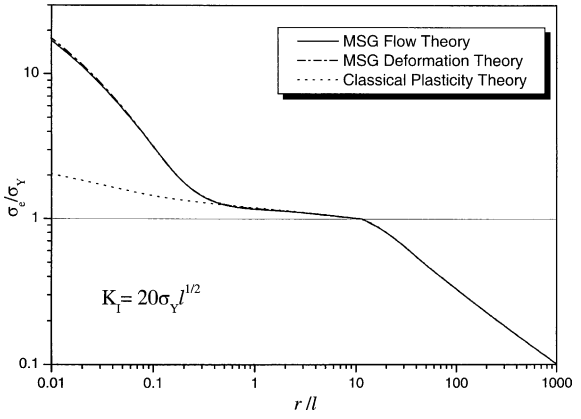


Fig. 3. The effective stress $\sigma_e$ normalized by the yield stress $\sigma_Y$ versus the normalized distance ahead of the crack tip, $r/l$, at polar angle $\theta = 1.014°$, where $l$ is the internal material length in strain gradient plasticity; plastic work hardening exponent $N = 0.2$, Possion's ratio $v = 0.3$, ratio of yield stress to elastic modulus $\sigma_Y/E = 0.2\%$, and remotely applied elastic stress intensity factor $K_I/\sigma_Y l^{1/2} = 20$; results are presented for flow and deformation theories of MSG plasticity, as well as for the classical flow theory of plasticity.

strain gradient plasticity (Fleck and Hutchinson, 1997). Outside the plastic zone, all three curves become the same straight lines with the slope of $-1/2$, corresponding to the elastic $K$ field with square-root singularity. Moreover, all three curves coincide inside the plastic zone at a distance of more than $0.3l$ away from the crack tip. With $l$ being 4 μm for copper (Fleck et al., 1994; Gao et al., 1999a), this means that the strain gradient effect is significant within a zone of more than 1 μm to the crack tip. This zone of 1 μm is still significantly larger than the average dislocation spacing around the crack tip (for a typical dislocation density of $10^{14}$ m$^{-2}$) such that continuum plasticity still applies. Within $0.3l$ to the crack tip, classical plasticity theory gives a straight line with the slope $-N/(N+1)$, corresponding to the HRR field (Hutchinson, 1968; Rice and Rosengren, 1968) in classical plasticity. Both flow and deformation theories of MSG plasticity show that the effective stress in MSG plasticity is much larger than that in classical plasticity. For example, at a distance of $0.1l$ to crack tip, which is approximately 0.4 μm for copper and is within the intended application range of MSG plasticity (Gao et al., 1999b; Huang et al., 2000a), the effective stress predicted by MSG plasticity more than doubles that in classical plasticity. It is also observed that the absolute value of the slope at each point on the curve for MSGplasticity exceeds or equals to $1/2$, suggesting the crack tip field in MSG plasticity is not only more singular than the HRR field, but also more singular than the elastic $K$ field. This high stress singularity results from the dominance of geometrically necessary dislocations around the crack tip in MSG plasticity (Shi et al., 2001).

Fig. 4 shows the distribution of normal stresses $\sigma_{\theta\theta}$ and $\sigma_{rr}$ ahead of the crack tip (at polar angle $\theta = 1.0143°$) predicted by both flow and deformation theories of MSG plasticity, as well as by the classical flow theory of plasticity. Material properties are given in (36), and the remote applied stress intensity factor is $K_I/\sigma_Y l^{1/2} = 20$. It is observed once again that the difference between two theories of MSG plasticity is very small. At a small distance $r$ to crack tip, normal stresses in MSG plasticity are larger than their counterparts in

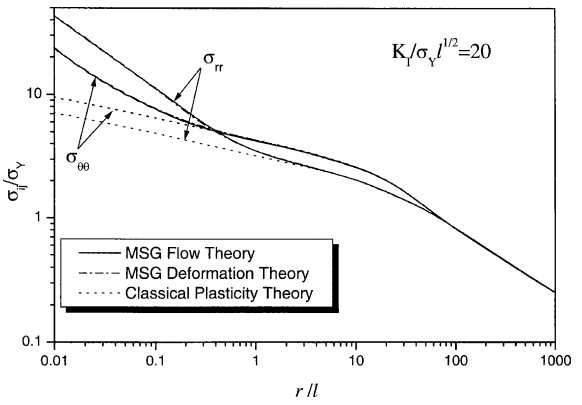


Fig. 4. The distribution of normal stresses $\sigma_{\theta\theta}$ and $\sigma_{rr}$ ahead of the crack tip (at polar angle $\theta = 1.014°$) for flow and deformation theories of MSG plasticity and for the classical flow theory of plasticity. All normalization and material and loading parameters are the same as those in Fig. 3.

classical plasticity, and are more singular than the HRR field or even the elastic $K$ field since the absolute value of the slope exceeds or equals to $1/2$.

Fig. 5 shows the normalized effective stress, $\sigma_e/\sigma_Y$, versus normalized distance ahead of the crack tip, $r/l$, at polar angle $\theta = 1.0143°$ for applied stress intensity factor $K_I/\sigma_Y l^{1/2} = 5$, 10, and 20. Results are presented for both flow and deformation theories of MSG plasticity, as well as

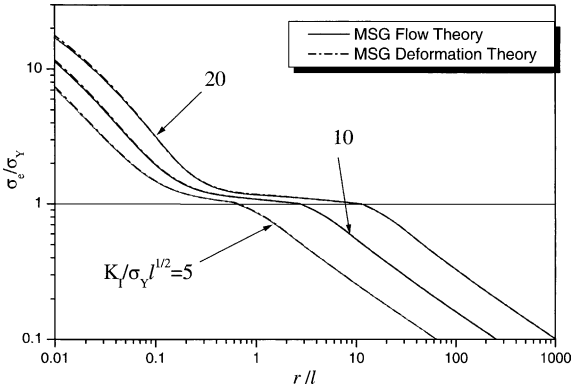


Fig. 5. The distribution of effective stress ahead of the crack tip (at polar angle $\theta = 1.014°$) for both flow and deformation theories of MSG plasticity. The remotely applied elastic stress intensity factor is $K_I/\sigma_Y l^{1/2} = 5$, 10 and 20. All normalization and material parameters are the same as those in Fig. 3.

for the classical flow theory of plasticity. Material properties are given in (36). It is observed once again that the difference between flow and deformation theories of MSG plasticity is vanishingly small, and the effective stress in MSG plasticity is significantly larger than that in classical plasticity near the crack tip. Similar to Fig. 3, the transition from the elastic $K$ field through a plastic zone to the near tip field in MSG plasticity is clearly observed, and the near-tip stress singularity in MSG plasticity is higher than the HRR field in classical plasticity as well as the elastic $K$ field. The plastic zone size increases rapidly with the applied load, as seen from the intercepts of all curves with the horizontal line $\sigma_e/\sigma_Y = 1$. Each curve within the plastic zone can be separated to a relatively flat portion and a portion that rises rather sharply near the crack tip, and the latter represents the dominance zone of the near-tip field in MSG plasticity. Even though the point separating the two portions is not rigorously defined, it is clear that the dominance zone size of the near-tip field in MSG plasticity increases much slower with the applied load than the plastic zone size does.

Fig. 6 shows the effect of plastic work hardening on the effective stress distribution ahead of the crack tip (at polar angle $\theta = 1.0143°$). The remote applied stress intensity factor is $K_I/\sigma_Y l^{1/2} = 20$, and plastic work hardening exponent $N = 0.1$, 0.2 and 0.3. It is observed that all curves seem to approach straight lines with the same slope at small distances to crack tip. This means the crack tip singularity in MSG plasticity, unlike that in the HRR field, is independent of the plastic work hardening exponent. The same conclusion has been established in the deformation theory of MSG plasticity (Jiang et al., 2001), and is consistent with Shi et al.'s (2000a, 2001) asymptotic analyses of crack tip field in MSG plasticity. In terms of dislocation terminologies, this means that the density of geometrically necessary dislocations is much higher than that of statistically stored dislocations near the crack tip.

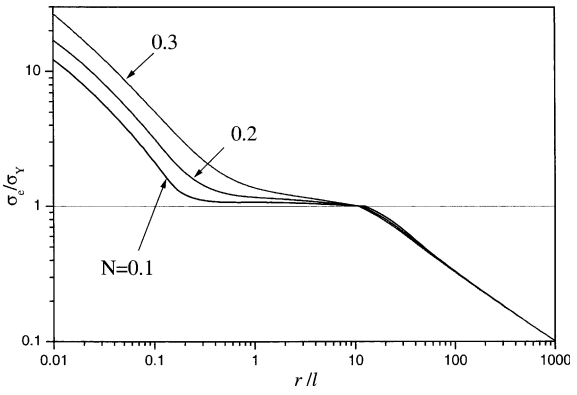


Fig. 6. The distribution of effective stress ahead of the crack tip (at polar angle $\theta = 1.014°$). All normalization and material and loading parameters are the same as those in Fig. 3, except the plastic work hardening exponent $N = 0.1$, 0.2 and 0.3.

The numerical studies in this section have confirmed the conclusion established by Jiang et al. (2001) that, due to the strain gradient effect, the stress level around a crack tip in MSG plasticity is significantly higher than its counterpart in classical plasticity. As discussed in detail in Jiang et al. (2001) and also in the next section, this provides an alternative approach to explain the cleavage fracture in ductile materials observed in experiments (Bagchi et al., 1994; Elssner et al., 1994; Bagchi and Evans, 1996).

## 5. Steady-state propagation of a mode-I crack

Recent experiments on metal-ceramic interfaces (Bagchi et al., 1994; Elssner et al., 1994; Bagchi and Evans, 1996) showed quasi-static propagation of interface decohesion cracks in presence of substantial plasticity in metals. The interface crack tips remained atomically sharp during continuous crack propagation even though the metallic constituents undergo significant plastic deformation. Elssner et al. (1994) measured both macroscopic fracture toughness and atomic work of separation of an interface between a single crystal niobium and a sapphire single crystal, and found that the macroscopic work of fracture was two to three orders of magnitude higher than the atomic work of separation. This large difference between the macroscopic work of fracture and its counterpart at the atomic level was attributed to plastic dissipation in niobium. This, however, leads to a "paradox" for continuum plasticity modeling of

cleavage or decohesion cracks. According to results from classical plasticity for growing plane-strain cracks in mode I, the maximum normal stress that can be attained ahead of the crack tip is about 2.6 times the initial tensile yield stress $\sigma_Y$ for an elastic-perfectly plastic solid (Drugan et al., 1982; Hwang and Luo, 1989). For a strain hardening solid, the stress level is higher, but the maximum normal stress never exceeds four to five times $\sigma_Y$ at relevant distances ahead of the crack tip (Gao and Hwang, 1981). On the other hand, atomic separation around a cleavage or decohesion crack requires a stress level on the order of theoretical lattice strength, which is roughly $E/30$, or 10 times $\sigma_Y$ for typical metals. The maximum stress ($4$–$5\sigma_Y$) predicted by classical plasticity clearly falls short to trigger atomic separation ($10\sigma_Y$) observed in experiments (Bagchi et al., 1994; Elssner et al., 1994; Bagchi and Evans, 1996).

Suo et al. (1993) proposed a model that embeds an elastic strip around the crack tip in order to provide the high stress level needed for an atomically sharp crack tip in ductile materials. The height of strip is on the order of dislocation spacing such that dislocation activities within the strip cannot be homogenized and characterized by continuum plasticity anymore. Such an elastic strip surrounded by a plastic zone indeed significantly increases the stress level near the crack tip. Beltz et al. (1996) extended Suo et al.'s (1993) model to provide a self-consistent estimate of the strip height based on dislocation analysis, and confirmed that the strip height is indeed on the order of dislocation spacing. Wei and Hutchinson (1999) combined Suo et al.'s (1993) model with the embedded cohesion surface approach (Needleman, 1987; Tvergaard and Hutchinson, 1992, 1993; Xu and Needleman, 1994; Camacho and Ortiz, 1996) to investigate the stress level around a crack tip.

Strain gradient plasticity may provide an alternative approach to explain the high stress level around a crack tip, as already demonstrated in the previous section for a stationary crack tip. In fact, using the phenomenological theory of strain gradient plasticity (Fleck and Hutchinson, 1997), Wei and Hutchinson (1997) have already shown that the normal stress traction ahead of a quasi-static, steadily growing mode-I crack is significantly elevated due to the strain gradient effect. The normal stress traction is much larger than its counterpart in classical plasticity, and has indeed reached the cleavage stress level of $10\sigma_Y$. Follow Wei and Hutchinson (1997), we use the flow theory of MSG plasticity to investigate steady state, quasi-static growth of a mode-I crack in this section. This is also a good example for the flow theory of MSG plasticity since the deformation theory is simply not applicable due to significant unloading during crack propagation.

The solution scheme for steady-state mode-I crack propagation in MSG plasticity is identical to that developed by Wei and Hutchinson (1997) for the phenomenological flow theory of strain gradient plasticity (Fleck and Hutchinson, 1997). Therefore, we do not present the solution scheme in this paper, and refer readers interested in the numerical method to Wei and Hutchinson (1997) for details. Similar to Wei and Hutchinson (1997), we focus on the normal stress distribution $\sigma_{22}(x)$ in the plane of crack propagation $y = 0$ ahead of the propagating crack tip, i.e.,

$$\frac{\sigma_{22}}{\sigma_Y} = f_{22}\left(\frac{x}{R_p}, \frac{l}{R_p}, N, \frac{\sigma_Y}{E}, \nu\right), \tag{37}$$

where $N$ is the plastic work hardening exponent, $\sigma_Y$ the yield stress, $E$ the elastic modulus, $\nu$ the Possion's ratio; $x$ the distance to the propagating crack tip, and the half height of plastic zone, $R_p$, is related to the remote applied elastic stress intensity factor $K_I$ by (Wei and Hutchinson, 1997)

$$R_p = \frac{K_I^2}{3\pi\sigma_Y^2}. \tag{38}$$

The ratio of internal material length $l$ to the half height of plastic zone $R_p$ in (37) is related to the normalized remote applied stress intensity factor $K_I/\sigma_Y l^{1/2}$ in (35) by

$$\frac{l}{R_p} = 3\pi\left(\frac{K_I}{\sigma_Y l^{1/2}}\right)^{-2}. \tag{39}$$

Fig. 7 shows the normalized stress distribution for $N = 0.2$, $\sigma_Y/E = 0.33\%$, $\nu = 0.3$, and $l/R_p = 0$, 1 and 2, where the limit $l/R_p = 0$ corresponds to the classical plasticity theory. It is observed that the strain gradient effect significantly increases the

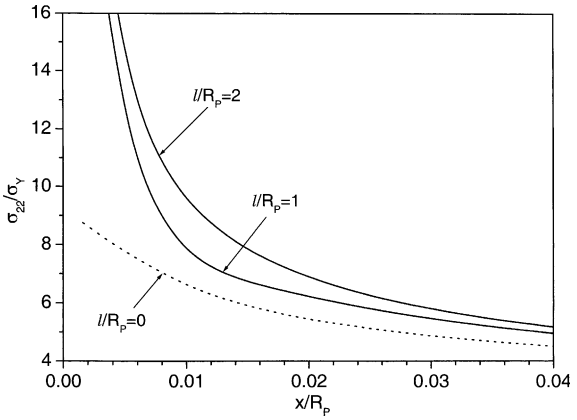


Fig. 7. The distribution of normal stress ahead of a steady state, quasi-statically growing crack tip, where $l$ is the internal material length in strain gradient plasticity; $R_p$ the half-height of plastic zone; plastic work hardening exponent $N = 0.2$, Possion's ratio $v = 0.3$, ratio of yield stress to elastic modulus $\sigma_Y/E = 0.33\%$. The limit $l/R_p = 0$ corresponds to classical plasticity without accounting for the strain gradient effect.

stress level ahead of the propagating crack tip, consistent with the conclusion established by Wei and Hutchinson (1997). Therefore, strain gradient plasticity indeed gives a much higher stress level than classical plasticity does, and provides an alternative approach to model cleavage or decohesion cracks in ductile materials. It should be pointed out that, at distances much further away from the crack tip, stresses in MSG plasticity drop slightly below those in classical plasticity. This was also observed by Wei and Hutchinson (1997), and is consistent with the requirement of overall force equilibrium that the higher stresses near the crack tip be offset by lower values away from the tip.

## 6. Summary

The following objectives have been achieved in this paper.

(i) The flow theory of MSG plasticity has been established via a multiscale, hierarchical framework to derive the mesoscale law of strain gradient plasticity from the microscale Taylor model in dislocation mechanics (Taylor, 1934, 1938).

(ii) Both flow and deformation theories of MSG plasticity agree very well with micro-indentation hardness experiments. The elastic compressibility (volumetric deformation) is important in the study of micro-indentation experiments and must be accounted for.

(iii) The flow theory of MSG plasticity agrees well with the deformation theory in the study of stationary crack tip field in MSG plasticity. The stress level around a crack tip in MSG plasticity is significantly larger than that in classical plasticity.

(iv) Crack propagation in elastic-plastic solids cannot be investigated by any deformation theories of plasticity because of significant unloading involved. The flow theory of MSG plasticity shows that the strain gradient effect significantly increases the stress level ahead of a steady state, quasi-statically propagating crack tip. This is consistent with Wei and Hutchinson's study (1997), and provides a means to explain the experimentally observed cleavage fracture in ductile materials (Bagchi et al., 1994; Elssner et al., 1994; Bagchi and Evans, 1996).

## Acknowledgements

YH acknowledges the support from US NSF (grant CMS-0084980 and a supplemental to grant CMS-9896285 from the NSF International Program). HG acknowledges the support from NSF (grant CMS-9979717). Support from NSFC is also acknowledged.

## References

Acharya, A., Bassani, J.L., 2000. Lattice incompatibility and a gradient theory of crystal plasticity. J. Mech. Phys. Solids 48, 1565–1595.

Acharya, A., Beaudoin, A.J., 2000. Grain-size effect in viscoplastic polycrystals at moderate strains. J. Mech. Phys. Solids 48, 2213–2230.

Aifantis, E.C., 1984. On the microstructural origin of certain inelastic models. Trans. ASME J. Eng. Mater. Technol. 106, 326–330.

Aifantis, E.C., 1992. On the role of gradients in the localization of deformation and fracture. Int. J. Eng. Sci. 30, 1279–1299.

Arsenlis, A., Parks, D.M., 1999. Crystallographic aspects of geometrically-necessary and statistically-stored dislocation density. Acta Mater. 47, 1597–1611.

Ashby, M.F., 1970. The deformation of plastically non-homogeneous alloys. Phil. Mag. 21, 399–424.

Atkinson, M., 1995. Further analysis of the size effect in indentation hardness tests of some metals. J. Mater. Res. 10, 2908–2915.

Bagchi, A., Evans, A.G., 1996. The mechanics and physics of thin film decohesion and its measurement. Interface Sci. 3, 169–193.

Bagchi, A., Lucas, G.E., Suo, Z., Evans, A.G., 1994. A new procedure for measuring the decohesion energy of thin ductile films on substrates. J. Mater. Res. 9, 1734–1741.

Begley, M.R., Hutchinson, J.W., 1998. The mechanics of size-dependent indentation. J. Mech. Phys. Solid 46, 2049–2068.

Beltz, G.E., Rice, J.R., Shih, C.F., Xia, L., 1996. A self-consistent model for cleavage in the presence of plastic flow. Acta Mater. 44, 3943–3954.

Camacho, G.T., Ortiz, M., 1996. Computational modeling of impact damage in brittle materials. Int. J. Solids Struct. 33, 2899–2938.

Cleveringa, H.H.M., van der Giessen, E., Needleman, A., 1997. Comparison of discrete dislocation and continuum plasticity predictions for a composite material. Acta Mater. 45, 3163–3179.

Cleveringa, H.H.M., van der Giessen, E., Needleman, A., 1998. Discrete dislocation simulations and size dependent hardening in single slip. J. Phys. IV 8, 83–92.

Cleveringa, H.H.M., van der Giessen, E., Needleman, A., 1999a. A discrete dislocation analysis of bending. Int. J. Plasticity 15, 837–868.

Cleveringa, H.H.M., van der Giessen, E., Needleman, A., 1999b. A discrete dislocation analysis of residual stresses in a composite material. Philos. Mag. A 79, 893–920.

Cleveringa, H.H.M., van der Giessen, E., Needleman, A., 2000. A discrete dislocation analysis of mode I crack growth. J. Mech. Phys. Solids 48, 1133–1157.

Cottrell, A.H., 1964. In: The Mechanical Properties of Materials. J. Willey, New York, p. 277.

Dai, H., Parks, D.M., 2002. Geometrically-necessary dislocation density in continuum crystal plasticity theory and FEM implementation (unpublished manuscript).

de Borst, R., Muhlhaus, H.B., 1992. Gradient-dependent plasticity: formulation and algorithmic aspects. Int. J. Numer. Meth. Eng. 35, 521–539.

de Guzman, M.S., Neubauer, G., Flinn, P., Nix, W.D., 1993. The rule of indentation depth on the measured hardness of materials. Mater. Res. Symp. Proc. 308, 613–618.

Drugan, W.J., Rice, J.R., Sham, T.-L., 1982. Asymptotic analysis of growing plane strain tensile cracks in elastic-ideally plastic solids. J. Mech. Phys. Solids 30, 447–473.

Elssner, G., Korn, D., Ruehle, M., 1994. The influence of interface impurities on fracture energy of UHV diffusion bonded metal-ceramic bicrystals. Scripta Metall. Mater. 31, 1037–1042.

Fleck, N.A., Hutchinson, J.W., 1993. A phenomenological theory for strain gradient effects in plasticity. J. Mech. Phys. Solids 41, 1825–1857.

Fleck, N.A., Hutchinson, J.W., 1997. Strain gradient plasticity. In: Hutchinson, J.W., Wu, T.Y. (Eds.), Advances in Applied Mechanics, vol. 33. Academic Press, New York, pp. 295–361.

Fleck, N.A., Muller, G.M., Ashby, M.F., Hutchinson, J.W., 1994. Strain gradient plasticity: theory and experiment. Acta Metall Mater. 42, 475–487.

Gao, H., Huang, Y., Nix, W.D., 1999a. Modeling plasticity at the micrometer scale. Naturwissenschaftler 86, 507–515.

Gao, H., Huang, Y., Nix, W.D., Hutchinson, J.W., 1999b. Mechanism-based strain gradient plasticity—I. Theory. J. Mech. Phys. Solids 47, 1239–1263.

Gao, Y.C., Hwang, K.C., 1981. Elastic–plastic fields in steady crack growth in a strain hardening material. In: Franois, D. (Ed.), Advances in Fracture Research, Proceedings of Fifth International Congress of Fracture. Pergamon Press, New York, pp. 669–682.

Gurtin, M.E., 2000. On the plasticity of single crystals: free energy, microforces, plastic-strain gradients. J. Mech. Phys. Solids 48, 989–1036.

Hao, S., Liu, W.K., Qian, D., 2000. Localization-induced band and cohesive model. J. Appl. Mech. 67, 803–812.

Huang, Y., Gao, H., Hwang, K.C., 1999. Strain-gradient plasticity at the micron scale. In: Ellyin, F., Provan, J.W. (Eds.), Progress in Mechanical Behavior of Materials, vol. III, pp. 1051–1056.

Huang, Y., Gao, H., Nix, W.D., Hutchinsion, J.W., 2000a. Mechanism-based strain gradient plasticity-II. analysis. J. Mech. Phys. Solids 48, 99–128.

Huang, Y., Xue, Z., Gao, H., Nix, W.D., Xia, Z.C., 2000b. A study of micro-indentation hardness tests by mechanism-based strain gradient plasticity. J. Mater. Res. 15, 1786–1796.

Hutchinson, J.W., 1968. Singular behavior at the end of a tensile crack in a hardening material. J. Mech. Phys. Solids 16, 13–31.

Hwang, K.C., Luo, X.F., 1989. Near-tip fields of growing cracks and resistance curves. Mech. Mater. 7, 271–278.

Jiang, H., Huang, Y., Zhuang, Z., Hwang, K.C., 2001. Fracture in mechanism-based strain gradient plasticity. J. Mech. Phys. Solids 49, 979–993.

Lasry, D., Belytschko, T., 1988. Localization limiters in transient problems. Int. J. Solids Struct. 24, 581–597.

Lloyd, D.J., 1994. Particle reinforced aluminum and magnesium matrix composites. Int. Mater. Rev. 39, 1–23.

Ma, Q., Clarke, D.R., 1995. Size dependent hardness in silver single crystals. J. Mater. Res. 10, 853–863.

McElhaney, K.W., Vlassak, J.J., Nix, W.D., 1998. Determination of indenter tip geometry and indentation contact area for depth-sensing indentation experiments. J. Mater. Res. 13, 1300–1306.

McLean, D., 1962. Mechanical Properties of Metals. John Wiley and Sons, New York.

Muhlhaus, H.B., Aifantis, E.C., 1991. A variational principle for gradient plasticity. Int. J. Solids Struct. 28, 845–857.

Nan, C.W., Clarke, D.R., 1996. The influence of particle size and particle fracture on the elastic/plastic deformation of metal matrix composites. Acta Mater. 44, 3801–3811.

Needleman, A., 1987. A continuum model for void nucleation by inclusion debonding. J. Appl. Mech. 54, 525–531.

Needleman, A., 2000. Computational mechanics at the mesoscale. Acta Mater. 48, 105–124.

Nix, W.D., 1989. Mechanical properties of thin films. Metall. Trans. 20A, 2217–2245.

Nix, W.D., 1997. Elastic and plastic properties of thin films on substrates nanoindentation techniques. Mater. Sci. Engr. A 234–236, 37–44.

Nix, W.D., Gao, H., 1998. Indentation size effects in crystalline materials: a law for strain gradient plasticity. J. Mech. Phys. Solids 46, 411–425.

Nye, J.F., 1953. Some geometrical relations in dislocated crystals. Acta Metall. Mater. 1, 153–162.

Poole, W.J., Ashby, M.F., Fleck, N.A., 1996. Microhardness of annealed and work-hardened copper polycrystals. Scripta Metall. Mater. 34, 559–564.

Rice, J.R., 1970. On the structure of stress–strain relations for time-dependent plastic deformation in metals. J. Appl. Mech. 34, 728–737.

Rice, J.R., 1971. Inelastic constitutive relations for solids: an internal-variable theory and its application to metal plasticity. J. Mech. Phys. Solids 19, 433–455.

Rice, J.R., Rosengren, G.F., 1968. Plane strain deformation near a crack tip in a power law hardening material. J. Mech. Phys. Solids 16, 1–12.

Saha, R., Xue, Z., Huang, Y., Nix, W.D., 2001. Indentation of a soft metal film on a hard substrate: strain gradient hardening effects. J. Mech. Phys. Solids 49, 1997–2014.

Shi, M., Huang, Y., Gao, H., Hwang, K.C., 2000a. Nonexistence of separable crack tip field in mechanism-based strain gradient plasticity. Int. J. Solids Struct. 37, 5995–6010.

Shi, M., Huang, Y., Hwang, K.C., 2000b. Plastic flow localization in mechanism-based strain gradient plasticity. Int. J. Mech. Sci. 42, 2115–2131.

Shi, M., Huang, Y., Jiang, H., Hwang, K.C., Li, M., 2001. The boundary layer effect on the crack tip field in mechanism-based strain gradient plasticity. Int. J. Fracture 112, 23–41.

Shu, J.Y., Fleck, N.A., 1999. Strain gradient crystal plasticity: size-dependent deformation of bicrystals. J. Mech. Phys. Solids 47, 292–324.

Shu, J.Y., King, W.E., Fleck, N.A., 1999. Finite elements for materials with strain gradient effects. Int. J. Numer. Meth. Eng. 44, 373–391.

Sluys, L.J., de Borst, R., Muhlhaus, H.B., 1993. Wave-propagation, localization and dispersion in a gradient-dependent medium. Int. J. Solids Struct. 30, 1153–1171.

Stelmashenko, N.A., Walls, M.G., Brown, L.M., Milman, Y.V., 1993. Microindentation on W and Mo oriented single crystals: an STM study. Acta Metall. Mater. 41, 2855–2865.

Stolken, J.S., Evans, A.G., 1998. A microbend test method for measuring the plasticity length scale. Acta Mater. 46, 5109–5115.

Suo, Z., Shih, C.F., Varias, A.G., 1993. A theory for cleavage cracking in the presence of plastic flow. Acta Metall. Mater. 41, 151–1557.

Suresh, S., Nieh, T.G., Choi, B.W., 1999. Nano-indentation of copper thin films on silicon substrates. Scripta Mater. 41, 951–957.

Taylor, G.I., 1934. The mechanism of plastic deformation of crystals. Proc. Roy. Soc. London A 145, 362–387.

Taylor, G.I., 1938. Plastic strain in metals. J. Inst. Met. 62, 307–324.

Tvergaard, V., Hutchinson, J.W., 1992. The relation between crack growth resistance and fracture process parameters in elastic-plastic solids. J. Mech. Phys. Solids 40, 1377–1397.

Tvergaard, V., Hutchinson, J.W., 1993. The influence of plasticity on mixed mode interface toughness. J. Mech. Phys. Solids 41, 1119–1135.

Tymiak, N.I., Kramer, D.E., Bahr, D.F., Wyrobek, T.J., Gerberich, W.W., 2001. Plastic strain and strain gradients at very small indentation depths. Acta Mater. 49, 1–14.

van der Giessen, E., Needleman, A., 1995. Discrete dislocation plasticity—A simple planar model. Model. Simul. Mater. Sci. 3, 689–735.

Wei, Y., Hutchinson, J.W., 1997. Steady-state crack growth and work of fracture for solids characterized by strain gradient plasticity. J. Mech. Phys. Solids 45, 1253–1273.

Wei, Y., Hutchinson, J.W., 1999. Models of interface separation accompanied by plastic dissipation at multiple scales. Int. J. Fracture 95, 1–17.

Xu, X.-P., Needleman, A., 1994. Numerical simulations of fast crack growth in brittle solids. J. Mech. Phys. Solids 42, 1397–1434.

Xue, Z., Huang, Y., Li, M., 2002a. Particle size effect in metallic materials: a study by the theory of mechanism-based strain gradient plasticity. Acta Mater. 50, 149–160.

Xue, Z., Saif, M.T.A., Huang, Y., 2002b. The strain gradient effect in micro-electro-mechanical systems (MEMS). J. Microelectromechanical Systems 11, 27–35.

Zbib, H.M., Aifantis, E.C., 1988. On the localization and postlocalization behavior of plastic deformation. Part I. On the initiation of shear bands; Part II. On the evolution and thickness of shear bands; Part III. On the structure and velocity of Portevin-Le Chatelier bands. Res. Mech. 23, 261–277, 279–292, and 293–305.

Zhu, H.T., Zbib, H.M., Aifantis, E.C., 1997. Strain gradient and continuum modeling of size effect in metal matrix composites. Acta Mech. 121, 165–176.